Inorganic Chemistry

Article

pubs.acs.org/IC

Sensitivity of Solvation Environment to Oxidation State and Position in the Early Actinide Period

Aurora E. Clark,*[,†] Alex Samuels,[†] Katy Wisuri,[†] Sarah Landstrom,[‡] and Tessa Saul[§]

[†]Department of Chemistry and the Materials Science and Engineering Program, Washington State University, Pullman, Washington 99164, United States

[‡]Department of Physics, Kutztown University, Kutztown, Pennsylvania 19530, United States

[§]Moscow High School, Moscow, Idaho 83843, United States

Supporting Information

ABSTRACT: The aqueous solvation of U−Pu in the III−VI oxidation states has been examined using density functional theory and hydrated cluster models of the form $An(H_2O)_{30}^{4+/3+}$ and $AnO_2(H_2O)_{30}^{2+/+}$ embedded within a polarizable continuum model to approximate the effect of bulk water. The structural features are compared to available data from extended X-ray absorption fine structure. Then, using a multiple-scattering approach, the X-ray absorption near-edge spectra (XANES) have been simulated and compared to experiment. These structural data are complemented by a detailed thermodynamic analysis using a recently benchmarked protocol. The structural, spectroscopic, and thermodynamic information has been used to assign the primary solvation environments in water, with an emphasis upon understanding how oxidation state and position in the period modifies the hydration number and equilibrium between different solvation shell environments. Tetravalent U is proposed to exist in equilibrium between the 8- and 9-coordinate species. Moving to the right of the period, Np(IV) and Pu(IV) exist solely as the octa-aquo species. Reduction to the trivalent ions leads to thermodynamic favorability for this solvation environment, whose features reproduce the XANES spectra. The actinyl dications (AnO_2^{2+}) of U and Np have a preferred environment in the equatorial plane consisting of 5 solvating waters; however, changes to the ionic radius and electronic structure at Pu leads to an equilibrium between the 4- and 5-coordinate species for PuO_2^{2+}. Reduction of the dications to form the monocations generally leads to a preference for the 4-coordinate primary solvation shell, with an equilibrium existing for uranyl, while the neptunyl and plutonyl species exist solely as $AnO_2(H_2O)_4^{+}$. These data provide accurate thermodynamic information for several rare species and the combined thermodynamic, structural, and spectroscopic approach reveals trends in hydration behavior across actinide oxidation states and within the early actinide period.

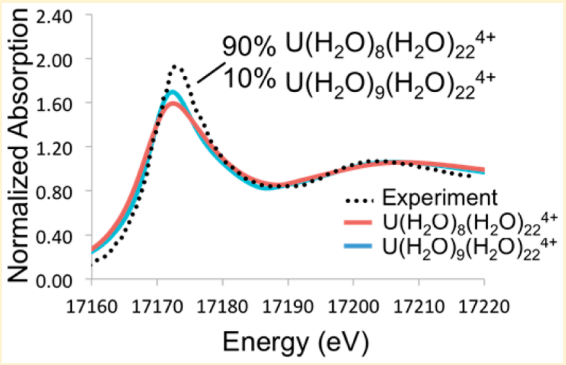

INTRODUCTION

The solvation environment about a metal cation has a practical impact upon reaction dynamics and understanding potentially complex speciation. Nowhere is this more apparent than in the early actinides (An), which includes U, Np, and Pu. Four common oxidation states exist for these species, III−VI, and *in situ* redox reactions (disproportionation and reproportionation) as well as radiolysis can cause remarkably complex chemistry, even in pure water.[1,2] Historically, significant experimental work has gone toward elucidating the aqueous hydration environment described by the coordination number (CN), polyhedral geometry adopted within the first solvation shell and the associated $An-OH_2$ bond distances of An(III−VI) under varying pH conditions (see, for example, refs 2−11 and references therein). Extended X-ray absorption fine structure (EXAFS), X-ray absorption near-edge spectroscopy (XANES), and other X-ray scattering methods (wide-angle, large-angle, high-energy) can provide first coordination shell structural data or pair correlations functions for all atoms in solution. However, interpretation of this data is often model-dependent, which can lead to inconsistent or contradictory reports. Indeed, the precision in an EXAFS measurement of the coordination number may vary within a few percent, yet the absolute accuracy may depend more on the modeling technique or the assumption of the CN.[12] Thermodynamic properties, such as the aqueous free energy of solvation (ΔG_{solv}), have been studied using calorimetry and imposing different ionic models.[1,13−17] However, the reported values have error bars larger than the differences in energy among varying solvation environments, and solution-phase conditions that stabilize a particular metal charge may also lead to unanticipated effects upon the data.

Given these experimental challenges, computational chemistry has been used to complement experiment and help assign the aqueous first salvation shell environments of actinides based

Received: February 16, 2015
Published: June 19, 2015

DOI: 10.1021/acs.inorgchem.5b00365
Inorg. Chem. 2015, 54, 6216−6225

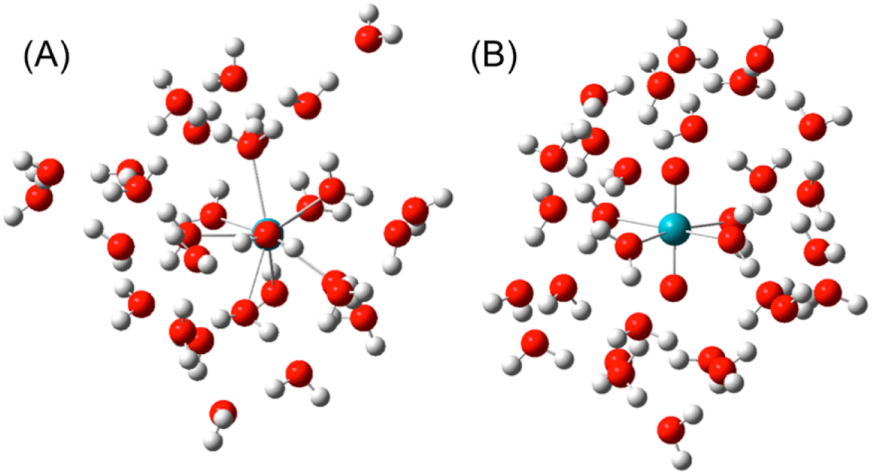

Figure 1. Representative UB3LYP/RSC60/6-311G** optimized geometries for the 1st and 2nd solvation shell structures (A) $An(H_2O)_9$-$(H_2O)_{21}^{3+/4+}$ and (B) $AnO_2(H_2O)_4(H_2O)_{26}^{1+/2+}$.

upon matching either structural, spectroscopic, and/or thermodynamic data. Often, a hydrated cluster consisting of a first solvation shell approximates the structure in solution;[5,18−26] however, a growing body of work has demonstrated the importance of a second solvation shell of explicit water molecules so as to describe polarization and charge transfer across solvation shells.[20,27−29] Density functional theory (DFT) is most commonly used, as it is practical from a resource perspective and relativistic effects can be taken into account as part of the method itself (for example, through the zero-order regular approximation − ZORA DFT) or in the description of the metal atomic orbitals (for example, using a relativistically corrected effective core potential − RECP − and its associated basis sets). Most works attempt to correlate computed data with a single set of experimental values, and in general, there have been few systematic studies across the actinide period and as a function of oxidations states using the same computational protocol. As such, there are still unassigned aqueous solvation environments for actinides in the (III−VI) oxidation states, and the energetic differences between solvation environments, which alter the Boltzmann distribution of observed configurations, are not generally discussed. Thus, there exist in the literature many isolated computational studies that use different methods, basis sets, and chemical models to investigate actinide solvation, making it is difficult to compare trends in solvation properties across oxidation states or the period.

In recent work, we have benchmarked the behavior and performance of different dielectric continuum models (and their cavities) for reproducing the free energies of solvation and water addition thermodynamics within different solvation environments of U(III−VI).[27] This has included a detailed accounting of error cancellation within large hydrated clusters of metal ions, allowing a computational protocol to be determined that was capable of determining accurate solution-phase thermochemical values across a broad range of cation charge. That work demonstrated that a polarizable continuum model (PCM) using the integral-equation-formalism protocol with a UFF cavity[30] (IEFPCM-UFF) and a solvation environment about the cation consisting of two solvation shells is consistently able to reproduce solution-phase free energies and known water addition thermodynamics across all of U(III−VI). This is in spite of the fact that UFF was originally parameterized for a single oxidation date. Using this approach, the focus of the current work is to now provide a consistent series of predicted thermodynamic, structural, and spectroscopic properties of solvated U, Np, and Pu across the III−VI oxidations states. The combined predicted properties are used to assign the primary aqueous solvation environments of An(III−VI), how they change across oxidation state and the 5*f* period, and to understand the energetic differences between first solvation structures, which helps to resolve prior inconsistencies in the literature that may be attributed to the effects of the solution-phase conditions upon equilibria between different coordination numbers in the first solvation shell (for example, refs 6, 31, and 32).

COMPUTATIONAL METHODS

The computational protocol employed has been validated in recent work that has compared the aqueous-phase thermochemistry of different PCM models and a variety of ways in which to construct the cavity about hydrated U(III−VI).[27] The geometries of large solvation shell clusters $An(H_2O)_{8,9}(H_2O)_{21,22}^{4+/3+}$ and $AnO_2(H_2O)_{4,5}$-$(H_2O)_{25,26}^{2+/+}$ (An = U, Np, Pu) have been optimized using the NWChem[33] software package (Figure 1). Prior work has illustrated the change in accuracy of these solution-phase thermochemical values as a function of the number of explicit waters used in hydrated clusters.[27] There, it was demonstrated that clusters with a second solvation shell of waters (as in the n = 30 case) optimized the cancellation of errors in the electrostatic and nonelectrostatic contributions to the free energy of solvation (reactions r1−r2). Within the specific clusters employed here, some optimized structures had 1−2 H_2O molecules migrate into a third solvation shell environment; however, it is very important to maintain a consistent number of H_2O across the entire reaction series (*vide infra*).

The unrestricted UB3LYP[34,35] combination of density functionals was employed during optimization, using the Stuttgart "small-core" RSC60 relativistic effective core potential (RECP) for all An, which replaces the 60 inner-shell ($[Kr]4d^{10}4f^{14}$) electrons with a pseudopotential.[36] The corresponding Stuttgart basis describes the valence electrons of An and consists of segmented contracted 8*s*7*p*6*d*4*f* functions. The 6-311G** basis set[37] was employed for the H and O atoms in these large hydrated cluster clusters. The complete basis set for the entire hydrated cluster is denoted by UB3LYP/RSC60/6-311G**. Frequency calculations were performed to obtain thermochemical corrections and ensure that structures correspond to local minima. All calculations neglected spin−orbit (SO) effects within the 5*f* subshell, as recent studies have demonstrated the effect of SO to be negligible.[27,38,39] The computation of the L_3-edge XANES spectra for the optimized hydrated clusters was carried out using the multiple-

DOI: 10.1021/acs.inorgchem.5b00365
Inorg. Chem. 2015, 54, 6216−6225

scattering code FEFF9,[40,41] following the methodology of Ankudinov et al. for Pu hydrates.[42] Details of the input parameters used in these calculations are described in the Supporting Information. Within this approach, and in the impending Results and Discussion section, it is important to note that the XANES simulation is quite sensitive to the construction of the muffin-tin potential, where the total electron density is approximated by overlapped free-atom densities. The relative edge of the white line is often underestimated, and as such, all simulated spectra were aligned to the maximum of the experimental white line (no other adjustments were performed).

Single-point IEFPCM-UFF calculations, as implemented in Gaussian 03,[43] were performed to account for the effects of the bulk solvent upon the computed thermodynamic parameters. The aqueous-phase solvation free energies (ΔG_{solv}) were calculated according to reactions

$$An^{4+/3+} + (H_2O)_{30} \rightarrow An(H_2O)_{8,9}(H_2O)_{22,21}{}^{4+/3+} \quad (r1)$$

$$AnO_2{}^{2+/+} + (H_2O)_{30} \rightarrow AnO_2(H_2O)_{4,5}(H_2O)_{26,25}{}^{2+/+} \quad (r2)$$

while the free energies of water addition (ΔG_{add}) were investigated using

$$An(H_2O)_8(H_2O)_{22}{}^{4+/3+} \rightarrow An(H_2O)_9(H_2O)_{21}{}^{4+/3+} \quad (r3)$$

$$AnO_2(H_2O)_4(H_2O)_{26}{}^{2+/+} \rightarrow AnO_2(H_2O)_5(H_2O)_{25}{}^{2+/+} \quad (r4)$$

The solvent-corrected free energies of these reactions are defined by

$$\Delta G_{rxn} = \Delta G_{gas}^{298} + \Delta G_{solv}^{tot} \quad (1)$$

which has ΔG_{gas}^{298} as the free energy of the reaction in the gas phase and ΔG_{solv}^{tot} as the solvation contribution to the free energy of the reaction (products minus reactants). A "standard state" correction, SS_{corr}, may also be applied to eq 1,[44,45] which is generally based upon the quasi-chemical method and is a measure of the reversible work of coupling the solute with the solvent (also referred to as the Ben-Naim definition). This correction amounts to $-4.3/n$ kcal/mol for each $(H_2O)_n$ water cluster and is thus quite small relative to the other two terms if a hydrogen-bonded cluster is employed, as in the current work. The use of a hydrogen-bonded water cluster also avoids imbalances in the hydrogen bond network of the reactants and products. While the clusters employed in reactions r1−r4 are rather large, an important factor to the effective cancellation of error in determining accurate ΔG_{solv} values is the specific maintenance of the same number of hydrogen bonds in the reactant and product clusters. This protocol enables a partial accounting of configurational sampling within the clusters because different configurations that have the same number of H bonds have very close energies. Counterpoise corrections were not included in eq 1 to correct for basis set superposition error, as prior studies have shown that the magnitude of the correction is minimal compared to water binding energies to trivalent lanthanides.[46] For instructive purposes, the implementation of the calculation of ΔG_{solv} in a thermochemical cycle is presented in Figure S1 in the Supporting Information. Where relevant to the discussion of structural trends, the electronic structure and bonding of each species was analyzed via natural population analysis[47,48] in Gaussian 09,[49] using the partitioning of the core/valence/Rydberg space for the An of *5s5p5d6s6p/5f6d7s7p/6f7d7f8s8p8d8f9s9p9d10s10p10d11s11p*.[50]

RESULTS AND DISCUSSION

The results are first presented for those systems for which the most is known experimentally, so as to further validate the aforementioned benchmarking study of the computational protocol,[27] and to obtain confidence in the proposed equilibria between solvation environments characterized by the different coordination numbers in the first solvation shell. Thereafter, trends in the change in solvation environment as a function of oxidation state and position in the 5f period are elucidated.

Tetravalent Actinide Ions. Because of a high electric charge, tetravalent An have a strong tendency toward hydrolysis in aqueous solution and can undergo polynucleation or colloidal formation.[51] The 4+ ions of U, Np, and Pu are also easily oxidized to the linear dioxo "yl" species. Experimental free energies of hydration have been determined for all of the tetravalent ions under study, and EXAFS has obtained average An−OH_2 bond lengths. However, the relative energies of different hydration numbers have not been discussed, and thus, it is unclear to what extent multiple coordination environments may be present in solution and whether these may be influenced by solution-phase conditions. In the case of hydration about U(IV), reported CN from electronic absorption, XANES, and EXAFS methods initially spanned 8−11.[5,52−57] However, more recent work, including B3LYP DFT and QM/MM studies of hydrated U(IV), have supported CN = 9, and *ab initio* molecular dynamics have reported an average coordination number of 8.7.[23,58,59] The most recent tetravalent Np studies have reported coordination numbers of 8 and 9 according to electronic absorption and EXAFS,[11,53] and similarly for Pu(IV).[12,42,53] Previous computational studies using B3LYP have not determined a preference for 8 or 9 water molecules in the first hydration sphere for Np(IV).[23] Computational studies regarding Pu(IV) hydration have employed B3LYP and PBE[60,61] density functionals and presumed an 8-coordinate first solvation shell.[25,62] Recent Car−Parrinello molecular dynamics simulations have also predicted the octa-aqua species.[64] The aqueous thermochemistry is first discussed, then the agreement of key bond lengths within the hydrated clusters to experiment is investigated, and, finally, we compare reported and simulated XANES spectra.

From a thermodynamic perspective, two quantities can be utilized for predicting the favored hydration environment: the free energy of solvation (ΔG_{solv}), and the energetics of water addition reactions in the first solvation shell (ΔG_{add}). The experimental ΔG_{solv} are known for all of the tetravalent ions in this work, which enables validation of the IEFPCM-UFF approach coupled with the second solvation shell cluster models. First, as observed in Table 1, it is important to note that at least one of the hydrated clusters (with either 8 or 9 H_2O in the first solvation shell) has a calculated free energy of solvation within the experimental error for all ions studied. With the exception of Pu^{4+}, the calculated ΔG_{solv} for the different coordination environments in the first solvation shell are quite close to each other, and thus, the data in combination with the typical experimental error of ±10 kcal/mol prevent distinction regarding the favorability of the 8- or 9-coordinate solvation environment in aqueous solution.

Inspection of Table 1 can yield the thermodynamics of the water addition reaction $An(H_2O)_8(H_2O)_{22}{}^{4+} \rightarrow An(H_2O)_9(H_2O)_{21}{}^{4+}$, wherein a second shell water migrates into the first shell. This data is also presented in Table 2, to provide clearer evidence regarding which species is thermodynamically favored. For these second solvation shell clusters, IEFPCM-UFF predicts a slight preference for the 8-coordinate species in tetravalent U (ΔG_{add} = 1.3 kcal/mol) and Np (ΔG_{add} = 2.7 kcal/mol), while there is significant thermodynamic favorability of $Pu(H_2O)_8(H_2O)_{22}{}^{4+}$ over $Pu(H_2O)_9(H_2O)_{21}{}^{4+}$ (ΔG_{add} = 12.5 kcal/mol). Given that the number of waters is maintained in the two clusters that have 8- vs 9-coordinate primary solvation environments, we can consider both as being reflective of different "states" of the same system. While an ensemble of configurations is not present for these two cases, it

DOI: 10.1021/acs.inorgchem.5b00365
Inorg. Chem. 2015, 54, 6216−6225

Table 1. UB3LYP/RSC60/6-311G IEFPCM-UFF Calculated ΔG_{solv} Values (in kcal/mol) for U, Np, and Pu in the III−VI Oxidation States, Calculated Using Reactions r1−r2 in Comparison to Experimental Data[1,13,64]**

An^{4+}		
	ΔG_{solv}	expt
$U(H_2O)_8(H_2O)_{22}^{4+}$	−1437.9	−1432.6 ± 10
$U(H_2O)_9(H_2O)_{21}^{4+}$	−1436.7	
$Np(H_2O)_8(H_2O)_{22}^{4+}$	−1450.5	−1446.0 ± 10
$Np(H_2O)_9(H_2O)_{21}^{4+}$	−1447.8	
$Pu(H_2O)_8(H_2O)_{22}^{4+}$	−1475.3	−1459.1 ± 10
$Pu(H_2O)_9(H_2O)_{21}^{4+}$	−1462.9	
An^{3+}		
	ΔG_{solv}	expt
$U(H_2O)_8(H_2O)_{22}^{3+}$	−766.9	−773.9 ± 10
$U(H_2O)_9(H_2O)_{21}^{3+}$	−761.6	
$Np(H_2O)_8(H_2O)_{22}^{3+}$	−773.1	−783.5 ± 10
$Np(H_2O)_9(H_2O)_{21}^{3+}$	−770.4	
$Pu(H_2O)_8(H_2O)_{22}^{3+}$	−786.3	−791.8 ± 10
$Pu(H_2O)_9(H_2O)_{21}^{3+}$	−781.1	
AnO_2^{2+}		
	ΔG_{solv}	expt
$UO_2(H_2O)_4(H_2O)_{26}^{2+}$	−387.4	−397 ± 15
$UO_2(H_2O)_5(H_2O)_{25}^{2+}$	−389.7	
$NpO_2(H_2O)_4(H_2O)_{26}^{2+}$	−542.2	
$NpO_2(H_2O)_5(H_2O)_{25}^{2+}$	−548.4	
$PuO_2(H_2O)_4(H_2O)_{26}^{2+}$	−532.4	
$PuO_2(H_2O)_5(H_2O)_{25}^{2+}$	−531.6	
AnO_2^{+}		
	ΔG_{solv}	expt
$UO_2(H_2O)_4(H_2O)_{26}^{+}$	−259.7	
$UO_2(H_2O)_5(H_2O)_{25}^{+}$	−260.8	
$NpO_2(H_2O)_4(H_2O)_{26}^{+}$	−300.2	
$NpO_2(H_2O)_5(H_2O)_{25}^{+}$	−256.2	
$PuO_2(H_2O)_4(H_2O)_{26}^{+}$	−486.1	
$PuO_2(H_2O)_5(H_2O)_{25}^{+}$	NA	

Table 2. UB3LYP/RSC60/6-311G Calculated ΔG_{add} Values (in kcal/mol) Using Reactions r3−r4**

reaction r3: $An(H_2O)_8(H_2O)_{22}^{4+} \rightarrow An(H_2O)_9(H_2O)_{21}^{4+}$			
	U	Np	Pu
ΔG_{add}	1.3	2.7	12.5
reaction r3: $An(H_2O)_8(H_2O)_{22}^{3+} \rightarrow An(H_2O)_9(H_2O)_{21}^{3+}$			
	U	Np	Pu
ΔG_{add}	5.4	2.7	5.3
reaction r4: $AnO_2(H_2O)_4(H_2O)_{26}^{2+} \rightarrow AnO_2(H_2O)_5(H_2O)_{25}^{2+}$			
	U	Np	Pu
ΔG_{add}	−2.3 (−2.1 to −2.5)[20]	−6.2	0.8
reaction r4: $AnO_2(H_2O)_4(H_2O)_{26}^{+} \rightarrow AnO_2(H_2O)_5(H_2O)_{25}^{+}$			
	U	Np	Pu
ΔG_{add}	−1.1	44.0	NA

is instructive to consider how the energy differences of the different coordination environments would impact the equilibrium between them. In this case, if we assume that the 8- and 9-coordinate species are the only configurations available to the actinide, then the energy differences between the states, ΔG_{add}, can be used to determine the equilibrium constant, and, in turn, to approximate the relative concentrations of these two solvation environments:

$$\frac{[An(H_2O)_8(H_2O)_{22}]^{4+}}{[An(H_2O)_9(H_2O)_{21}]^{4+}} = e^{\Delta G_{add}/kT} \quad (2)$$

As observed in Table 3, the small value of ΔG_{add} for tetravalent U leads to a left shifted equilibrium for reaction r3,

Table 3. Approximate Relative Concentrations of the Different Primary Solvation Environments of $An(H_2O)_{8,9}(H_2O)_{22,21}^{4+/3+}$ and $AnO_2(H_2O)_{4,5}(H_2O)_{26,25}^{2+/+}$, As Determined Using ΔG_{add} and eq 2 at a Temperature of 298 K

relative concentration	U	Np	Pu
% $An(H_2O)_8(H_2O)_{22}^{4+}$	90	99	100
% $An(H_2O)_9(H_2O)_{21}^{4+}$	10	1	0
% $An(H_2O)_8(H_2O)_{22}^{3+}$	100	99	100
% $An(H_2O)_9(H_2O)_{21}^{3+}$	0	1	0
% $AnO_2(H_2O)_4(H_2O)_{26}^{2+}$	2	0	79
% $AnO_2(H_2O)_5(H_2O)_{25}^{2+}$	98	100	21
% $AnO_2(H_2O)_4(H_2O)_{26}^{+}$	13	100	100
% $AnO_2(H_2O)_5(H_2O)_{25}^{+}$	87	0	0

favoring the 8-coordinate solvation environment (which will be present ∼90% of the time in solution) over the 9-coordinate environment (which will be present ∼10% of the time). The results for U(IV) contrast the conclusions drawn by Tsushima and co-workers,[23] who found a thermodynamic preference for the 9-coordinate species. Yet it is important to note that, while those calculations used a comparable method and basis set, symmetry was imposed during geometry optimization and the cluster model employed consisted of only a single solvation shell and used IEFPCM with the UA0 cavity rather than UFF, which we have demonstrated as having very poor agreement with experiment in the calculation of ΔG_{solv} using that cluster size.[27] The equilibrium nature of the 8- and 9-coordinate solvation environments determined here supports the observation of a noninteger CN in the *ab initio* molecular dynamics simulation fo U(IV),[59] where an average CN of 8.7 was observed at 300 K (within an ∼20 ps time scale). In the case of Np(IV) and Pu(IV), only the 8-coordinate environment should be observed at 298 K. This interpretation agrees well with Tsushima's studies of Np(IV) as well as recent Carr−Parrinello MD simulations of aqua Pu(IV).[23,63]

Comparison of calculated and experimental structural data as well as XANES spectra also reinforces the thermodynamic predictions from the large hydrated clusters. As seen in Table 4, the calculated r_{An-OH_2} distances in the first solvation shell are within the 0.01 Å error of the reported bond lengths from EXAFS and neutron diffraction methods.[11,12,65] In recent years, data treatments that enable effective background removal have improved the utility of high-energy X-ray scattering (HEXS) to probe the CN of actinide ions.[2] Yet, the polyhedral arrangement and extended solvation structure is better compared to results from XANES. Within this method, a Fourier transform of the X-ray absorption spectrum results in a radial distribution function that can be interpreted as shells of nearest-neighbor atoms surrounding the central ion. The position and intensity of the peaks in the Fourier transform are related to the atomic identity, distance, and number of atoms in each shell. Thus, XANES is sensitive to the bond angles the solvating H_2O adopt

DOI: 10.1021/acs.inorgchem.5b00365
Inorg. Chem. 2015, 54, 6216−6225

Table 4. Average UB3LYP/RSC60/6-311G $\langle r_{An-O}\rangle$ Bond Lengths (in Å) for $An(H_2O)_{8,9}(H_2O)_{21,22}^{4+}$ and $An(H_2O)_{8,9}(H_2O)_{21,22}^{3+}$ in Comparison with Experimental Values (in Parentheses). Average Charge Determined by NPA for the Metal Center and O Atoms Associated with the Inner-Sphere (IS) and Outer-Sphere (OS) Water Molecules Are Also Presented**

	$\langle r_{An-O}\rangle$ (expt)	CN_{expt}	q_{An}	$\langle q_O\rangle$ (IS)	$\langle q_O\rangle$ (OS)
$U(H_2O)_8(H_2O)_{22}^{4+}$	2.41 (2.42 ± 0.01[a])	9	1.96	−0.98	−1.03
$U(H_2O)_9(H_2O)_{21}^{4+}$	2.43		1.87	−0.96	−1.03
$Np(H_2O)_8(H_2O)_{22}^{4+}$	2.38 (2.37 ± 0.02[b])	9	1.86	−0.96	−1.03
$Np(H_2O)_9(H_2O)_{21}^{4+}$	2.40 (2.39 ± 0.01[b])	11	1.79	−0.96	−1.03
$Pu(H_2O)_8(H_2O)_{22}^{4+}$	2.39		1.64	−0.94	−1.03
$Pu(H_2O)_9(H_2O)_{21}^{4+}$	2.40 (2.39[a])	9	1.50	−0.93	−1.03
	$\langle r_{An-O}\rangle$	CN_{expt}			
$U(H_2O)_8(H_2O)_{22}^{3+}$	2.54 (2.56 ± 0.01[c])	9−10	1.83	−1.01	−1.04
$U(H_2O)_9(H_2O)_{21}^{3+}$	2.56		1.71	−1.01	−1.03
$Np(H_2O)_8(H_2O)_{22}^{3+}$	2.52 (2.48 ± 0.02[b])	8−10	1.84	−0.99	−1.03
$Np(H_2O)_9(H_2O)_{21}^{3+}$	2.57 (2.52 ± 0.01[c])	9	1.77	−1.01	−1.03
$Pu(H_2O)_8(H_2O)_{22}^{3+}$	2.50		1.63	−0.99	−1.04
$Pu(H_2O)_9(H_2O)_{21}^{3+}$	2.54 (2.51 ± 0.01[b])	9	1.47	−0.98	−1.03

[a]Reference 12. [b]Reference 60. [c]Reference 65.

about the actinide ion and the unique polyhedral geometry of the first solvation shell.[2] It can thus (in principle) distinguish between first solvation shells that are 8-coordinate and adopt a square antiprism geometry versus the 9-coordinate tricapped trigonal bipyramidal structure. It is important to note the solution-phase conditions of the previously reported XANES spectra of the early actinide ions. In general, for tetra- and trivalent ions, experimental conditions for X-ray scattering have metal concentrations between 0.01 and 0.05 M in dilute acid (often perchloric acid) of ∼0.1 molarity.[2]

Figure 2 presents the simulated XANES spectra of $An(H_2O)_8(H_2O)_{22}^{4+}$ and $An(H_2O)_9(H_2O)_{21}^{4+}$ overlaid with experiment[10,31] and contains inset tables with the root-mean-square error (RMSE) within different spectral regions. In the case of U(IV), the nona-aqua species has the best agreement with the edge of the white line; however, the octa-aqua species has the least error in the peak position and height, and in the high-energy feature. This further supports the conclusions that U(IV) likely exists in equilibrium with contributions of both species in solution to the XANES spectra. Indeed, a linear combination of the two spectra, weighted according to the theoretically predicted % contribution of each species, leads to slight improvements (<5%) in the RMSE values across the spectrum. However, it is important to note that the fundamental models employed to simulate the XANES spectrum are not equally accurate for all of the features present (peak onset, peak height, and the high-energy feature). Thus, one should not construe that a mere minimization of the RMSE between the two spectra and the experimental spectrum would yield accurate speciation of the different coordination environment. Rather, the data here should be viewed purely to support the proposal that a mixture of species is present.

In the case of Np(IV), the octa-aqua ion has significantly better agreement with the white line edge, though the peak positions, height, and the high-energy feature are essentially equally well-described by both 8- and 9-coordinate species. The simulated Np(IV) data contrast somewhat with conclusions drawn by Chaboy and co-workers,[52] who, using first solvation shell clusters obtained from the work of Tsushima et al.,[23] found better agreement with the experimental XANES spectra using a 9-coordinate tricapped trigonal bipyramical structure. We were unable to reproduce the unique structural features

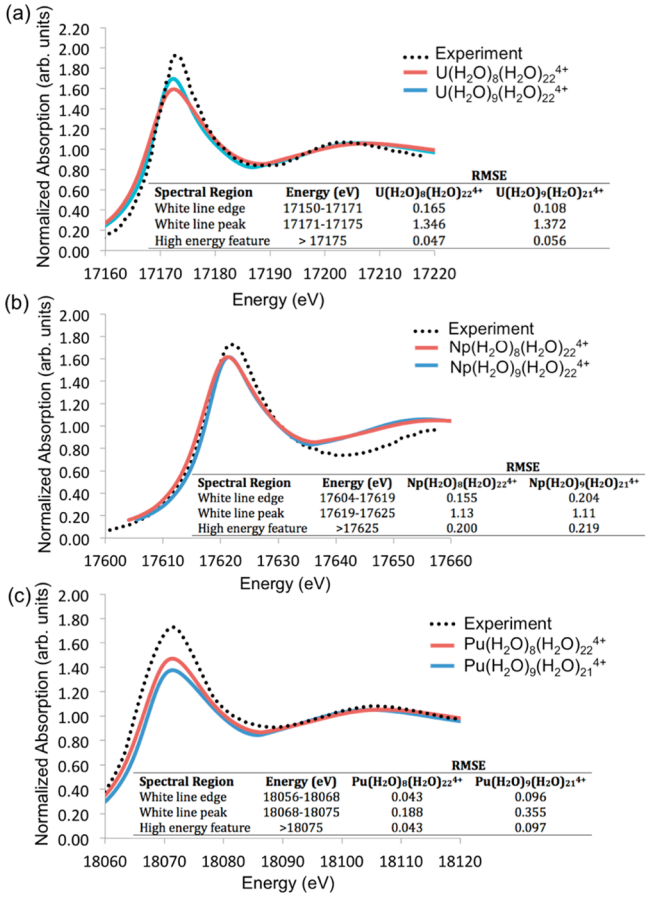

Figure 2. Simulated and experimental[10,31] XANES spectra of UB3LYP/RSC60/6-311G** optimized $An(H_2O)_{8,9}(H_2O)_{22,21}^{4+}$: (A) U, (B) Np, (C) Pu. The theoretical spectra have only been aligned to the maximum of the white line; no other shifting was performed.

observed within the simulated XANES spectra of the square antiprismatic structure utilized by Chaboy et al. using any of our hydrated clusters, and thus, it is unclear where this discrepancy may arise. In the discussion of aqueous Pu(IV), it is very apparent that the 8-coordinate first solvation shell has the closest agreement with the entire experimental spectrum,

DOI: 10.1021/acs.inorgchem.5b00365
Inorg. Chem. 2015, 54, 6216−6225

clearly indicating alongside the thermodynamic data that it is the predominant species in aqueous solution. In combination, the thermodynamic, structural, and spectroscopic features provide consistent and compelling evidence for equilibrium between the 8- and 9-coordinates solvation environments for U(IV), with the 8-coordinate species solely existing in solution at 298 K as you move to the right along the period for Np(IV) and Pu(IV).

Trivalent Actinide Ions. Trivalent U, Np, and Pu ions are obtained under acidic conditions at ~pH 0 within non-complexing media.[2] The specific CNs have been a subject of some debate experimentally, with 9−10 reported for U and Np, and 8−10 waters of hydration for Pu(III) (see ref 2 and references therein). Prior to 2007, there were few computational studies;[11,18,66] however, at that time, a comprehensive thermodynamic investigation using DFT and Møller−Plesset perturbation theory provided strong evidence that trivalent U, Np, and Pu likely exist with 8 waters in their first solvation shell.[67] This, in turn, has very recently been followed using coupled clusters with single-, double-, and perturbatively treated triple-excitations (CCSD(T)).[26] Clusters based upon a primary solvation environment were utilized in conjunction with a single continuum method to approximate the effects of the bulk, and no comparisons to spectroscopic data were made. The aforementioned convergence properties of the PCMs with the trivalent ions in conjunction with simulated XANES spectra provided herein help to solidify our understanding of the solvation behavior of these species.

Table 1 presents the calculated and experimental free energies of hydration of $An(H_2O)_{8,9}(H_2O)_{22,21}^{3+}$clusters, wherein at least one of these species has a free energy of solvation within the experimental error. Reduction of the tetravalent ion decreases the free energy of solvation by 47%, as would be anticipated by a simple Born model of a point charge in a spherical cavity, which approximates the decrease of the ion−dipole interactions in the first solvation shell. This is manifested in several ways, not the least of which is the decrease in total electron donation from the solvating waters 2.23 e^- to 1.29 e^- (Table 4). The thermodynamics of water addition reveals the preference for the 8-coordinate solvation environment for all ions studied (Table 2), in agreement with the previous thermodynamics assessments using DFT and recent *ab initio* MD studies.[63] For each ion, the free energy of water addition is such that calculation of the equilibrium constant reflects solely the 8-coordinate species being present in solution (Table 3). The structural and spectroscopic data further support these data. Reduction of An(IV) to An(III) leads to an increase in the average bond lengths that is in excellent agreement with experimental data (Table 4). Prior EXAFS study has shown that, for the oxidation of Np(III) to Np(IV) aquo ions, elongation of 0.11 Å in the average Np−O bond lengths from 2.37(1) to 2.48(2) Å, is observed.[11] The predicted contraction in the analogous reduction process is nearly identical at 0.12 Å.

To our knowledge, no XANES data have been reported for aqueous U(III); however, as seen in Figure 3, distinct spectral signatures are observed for the square antiprism (SAP) first solvation shell within $U(H_2O)_8(H_2O)_{22}^{3+}$ versus the tricapped trigonal bipyramid (TTBP) $U(H_2O)_9(H_2O)_{21}^{3+}$. The latter is observed to have significantly more intensity in the white line peak, with a spacing between that and the high-energy feature of 37 eV. In contrast, the SAP structure has an interpeak separation of 31 eV. In both the Np(III) and Pu(III) systems,

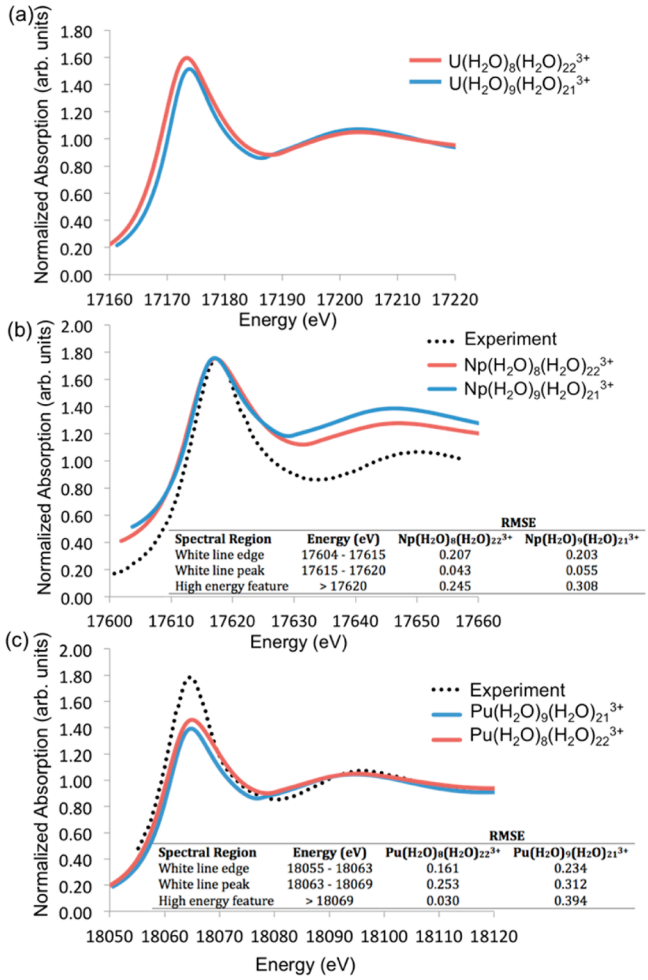

Figure 3. Simulated and experimental[10,31] XANES spectra of the UB3LYP/RSC60/6-311G** optimized $An(H_2O)_{8,9}(H_2O)_{22,21}^{3+}$: (A) U, (B) Np, (C) Pu. The theoretical spectra have only been aligned to the maximum of the white line (for Np(III) and Pu(III)); no other shifting was performed.

the simulated XANES spectrum of the cluster with 8 primary solvating waters is in best agreement with experiment.[10,31] The Pu(III) experimental spectrum was obtained using 0.05 M electrochemically produced Pu(III) from a Pu(VI) solution in 1 M perchloric acid.[32] There, approximately 8 waters were inferred in the first solvation shell; however, it was noted that the Pu(III) spectrum may be highly sensitive to the solution-phase conditions, as the use of a 0.02 M Pu(III) solution in 10 mM LiCl resulted in a primary solvation environment with 10 waters in the first solvation shell.[10] In combination, the thermodynamic, structural, and spectroscopic data strongly support 8-coordinate solvation environments for all trivalent early actinides, presumably in experimental environments where the effects of counterions are negligible, as implied by the second solvation shell hydrated clusters employed in this work.

Aqueous AnO_2^{2+} Ions. The An(VI) oxidation states are experimentally observed in near neutral pH and under slightly basic conditions.[2] As linear dioxo cations, they have unique hydration properties associated with the directed ligation of water into the equatorial plane. The UO_2^{2+} cation, due to its oxidation state stability, has been extensively studied by experiment and computation. Its hydration number was a

DOI: 10.1021/acs.inorgchem.5b00365
Inorg. Chem. 2015, 54, 6216−6225

Table 5. Average Equatorial, $\langle r_{An-OH_2}\rangle$ and Average Axial Metal−Oxygen Bond Lengths, $\langle r_{An=O}\rangle$, in (Å) for $AnO_2(H_2O)_{4,5}(H_2O)_{26,25}^{2+}$ and $AnO_2(H_2O)_{4,5}(H_2O)_{26,25}^{+}$ in Comparison with Experimental Values (in Parentheses). Average Charges (q) Are Reported, Determined by NPA for the Metal Center, Actinyl Oxo-Atom, O Atoms Associated with the Inner-Sphere (IS) and Outer-Sphere (OS) Water Molecules

	$\langle r_{An=O}\rangle$ (expt)	CN_{expt}	$\langle r_{An-OH_2}\rangle$ (expt)	q_{An}	$\langle q_{An=O*}\rangle$	$\langle q_O$ (IS)$\rangle$	$\langle q_O$ (OS)$\rangle$
$UO_2(H_2O)_4(H_2O)_{26}^{2+}$	1.77		2.36	1.70	−0.48	−0.94	−1.03
$UO_2(H_2O)_5(H_2O)_{25}^{2+}$	1.78 (1.76[a])	5	2.42 (2.41[a])	1.61	−0.49	−0.94	−1.03
$NpO_2(H_2O)_4(H_2O)_{26}^{2+}$	1.76		2.35	1.44	−0.37	−0.92	−1.03
$NpO_2(H_2O)_5(H_2O)_{26}^{2+}$	1.76 (1.75[b])	5	2.41 (2.41[b])	1.35	−0.39	−0.92	−1.03
$PuO_2(H_2O)_4(H_2O)_{26}^{2+}$	1.74		2.35	1.30	−0.32	−0.91	−1.03
$PuO_2(H_2O)_5(H_2O)_{26}^{2+}$	1.74 (1.74[c])	5−6	2.43 (2.45[c])	1.24	−0.32	−0.92	−1.03
	$\langle r_{An=O}\rangle$ (expt)	CN_{expt}	$\langle r_{An-OH_2}\rangle$ (expt)				
$UO_2(H_2O)_4(H_2O)_{26}^{+}$	1.84		2.48	1.70	−0.73	−0.99	−1.03
$UO_2(H_2O)_5(H_2O)_{25}^{+}$	1.85		2.49	1.65	−0.76	−0.97	−1.03
$NpO_2(H_2O)_4(H_2O)_{26}^{+}$	1.83 (1.822[b])	4	2.49 (2.488[b])	1.59	−0.64	−0.99	−1.03
$NpO_2(H_2O)_5(H_2O)_{26}^{+}$	1.84 (1.85[a])	5	2.51 (2.50[a])	1.48	−0.70	−0.96	−1.02
$PuO_2(H_2O)_4(H_2O)_{26}^{+}$	1.80 (1.84[d])	4	2.46 (2.45[d])	1.44	−0.59	−0.97	−1.03

[a]Reference 6. [b]Reference 31. [c]Reference 72. [d]Reference 12.

point of contention for several years; however, the most recent experimental data of UO_2^{2+} (using X-ray scattering methods in dilute acid solutions)[7] have supported the 5 H_2O case, which has been further bolstered by extensive computational studies utilizing DFT and other methods, such as MP2, CASSCF, CASPT2, CCSD, and CCSD(T).[68−71] There is larger uncertainly regarding hexavalent Np and Pu. Experimental EXAFS and XANES studies of 0.05 M Pu(VI) in nitric acid have inferred an equatorial CN of 4.4 ± 0.2, indicating a potential equilibrium between 4 and 5 waters in the equatorial plane.[31] Other experimental data have pointed to a CN of 5 in the equatorial plane for NpO_2^{2+} and 5 or 6 for PuO_2^{2+}.[31,72] The latter value is somewhat problematic because an increase in number of waters in the first solvation shell would not be anticipated due the actinide contraction, wherein the ionic radius decreases from 0.73 Å in U(VI) to 0.72 Å in Np(VI) to 0.71 Å in Pu(VI).[73] Many computational studies have assumed a 5-coordinate first solvation shell structure for Np(VI) and Pu(VI) and found good agreement between the structural and electronic properties (bond lengths, redox potentials, etc.) of these species and experiment.[2]

As observed in Table 1, the free energies of solvation for uranyl with either 4 or 5 waters in the equatorial plane are very close to the experimentally determined value of −397 kcal/mol and within the experimental error of ±15 kcal/mol. Note that these free energies, using a complete second solvation shell and the benchmarked PCM approach, are on the lower end of the experimental error, while prior calculations using a partial second solvation shell and MP2 had resulted in −410 kcal/mol, on the upper end of the experimental error.[20] As observed in Table 2 for UO_2^{2+}, IEFPCM-UFF predicts a free energy for water addition to the 4-coordinate species to create $UO_2(H_2O)_5(H_2O)_{25}^{2+}$ of −2.3 kcal/mol, in excellent agreement with prior studies by Gutowski and Dixon using MP2 and a benchmarked PCM approach.[20] Water addition to form the $NpO_2(H_2O)_5H_2O)_{25}^{2+}$ species is also predicted to be favorable, and thus, the equilibrium constant for both tetravalent U and Np indicates solely the 5-coordinate species in solution (Table 3). In the case of plutonyl, the very small positive ΔG_{add} leads to a predicted left-shifted equilibrium for reaction r4, wherein ∼79% of all species would be 4-coordinate and ∼21% would have 5 waters in the equatorial plane.

Prior simulation studies of the XANES spectra of actinyls have noted that the quantitative reproduction of the experimental spectrum is quite difficult.[42] Interestingly, inclusion of the H atoms in the cluster model employed generally decreases the instensity of the white line and yields larger disagreement with the experimental spectrum. This problem may be related to the construction of the muffin-tin potential. In either case, the simulated XANES spectra of the $AnO(H_2O)_{4,5}(H_2O)_{26,25}^{2+}$ clusters exhibit qualitative agreement with the experimental spectra, but present the aforementioned decreased intensity of the white line. Moreover, the simulated XANES spectra of the linear dioxo cations do not readily distinguish between the two coordination environments (4 or 5 waters in the equatorial plane) because the angular differences in the first solvation shell are modest: consisting of only an 18° change in the $\angle OH_2-An-OH_2$ (Figure S2 in the Supporting Information). This is in contrast to the differences between the SAP and TTBP geometries found in the aqueous $An^{4+/3+}$ species, which consisted of large variations in both $\angle OH_2-An-OH_2$ and also dihedral angles. Given the inconsistentices in the peak height intensities and the general similarity of the simulated spectra, the comparison of predicted and experimental XANES spectra are not employed in the discussion of the diyl cation solvation environments.

The thermodynamic preference of the penta-aqua solvation shell for uranyl and neptunyl is further supported by the close agreement of the calculated bond lengths to those reported from EXAFS studies (Table 5). However, structurally, the most consistent data with experiment for PuO_2^{2+} appear in the $PuO_2(H_2O)_5(H_2O)_{25}^{2+}$ species. The average An=O distances, $\langle r_{An=O}\rangle$, in all clusters reveal a systematic decrease in distance as one moves from U, to Np, to Pu. Interestingly, the reported ionic radii for these ions fit a linear function, while, in the calculated changes in bond distance from U to Pu, it appears that the contraction in the diyl Pu=O bond is more than would be expected from the actinide contraction alone. Investigation of the average actinide−water bond distance reveals the best agreement with the experimental values when there are 5 waters in the equatorial plane about U, Np, and Pu, having an average deviation of only 0.015 Å. These data are reflective of the slight increase in 6*d* atomic orbital energies and decrease in the 5*f* orbital energies that occur moving from U to

DOI: 10.1021/acs.inorgchem.5b00365
Inorg. Chem. 2015, 54, 6216−6225

Pu, which, in turn, increase the charge donation across the diyl bond. As seen in Table 5, the average charge of the diyl oxo-atoms in $AnO_2(H_2O)_5(H_2O)_{25}^{2+}$ is −0.41, meaning that 1.59 electrons are donated per oxo-atom (which are formally 2−) to the 6+ metal center. Moving from U to Pu results in a 35% increase in charge donation from the diyl-oxo to the actinide. These added electrons are donated primarily into the 5*f* orbitals, where the 5*f* electron configuration is $5f^{2.61}$ in $UO_2(H_2O)_5(H_2O)_{25}^{2+}$ and $5f^{4.94}$ in $PuO_2(H_2O)_5(H_2O)_{25}^{2+}$. This is ∼0.3 electrons more than anticipated based upon the fact that Pu(VI) formally has two more *f*-electrons than U(VI). Commensurate with the enhanced electron donation by the diyl oxo-atoms is a slight increase in the total electron donation to the metal from the solvating waters. In fact, the same changes in the electron donation of the solvating water are observed in the tetra- and trivalent ions as well. This electronic structure argument has been previously discussed in some detail within refs 69 and 70. In combination, the thermodynamic, geometric, and electronic structure information provides clear support of UO_2^{2+} and NpO_2^{2+} having 5 waters in the first solvation shell; however, it is likely that an equilibrium does occur for PuO_2^{2+}, though the very small energy associated with ΔG_{add} implies that the relative populations of tetra- and penta-aqua species may be highly influenced by temperature and experimental conditions.

Aqueous AnO_2^+ Ions. Though U(V) cations are highly reactive and readily disproportionate to formal IV and VI oxidation states,[2,74,75] NpO_2^+ and PuO_2^+ have been observed in acidic conditions.[2,76] Experimental studies have indicated the dioxo monocations to have 4−6 waters in the first solvation shell.[2] In the gas phase, AnO_2^+ hydrates have been recently produced by electrospray ionization, wherein only 4 H_2O were found in the first solvation shell.[77] To our knowledge, no experimental free energies of hydration exist for any of the 1+ diyl cations and water addition reactions have only recently been studied using a single solvation shell in the gas phase (for comparison to the reported electrospray data). As observed in Table 1, reduction of UO_2^{2+} and NpO_2^{2+} leads to a 30−50% reduction in ΔG_{solv}. This would be anticipated, as the decreased charge on the actinyl unit, in turn, decreases the strength of the ion−dipole interaction with water, as evidenced by the 40% decrease in the electron donation from the solvating waters to the cation. The affect of reduction upon the ΔG_{solv} is consistent with that observed in the 4+ → 3+ reduction; however, unlike the hard sphere ions, it is not quantitatively described by the Born model as the actinyl is not a simple point charge.

As seen in Table 2, the IEFPCM-UFF implementation predicts the value of ΔG_{add} to form $UO_2(H_2O)_5(H_2O)_{25}^+$ from the 4-water equatorial species to be −1.1 kcal/mol, and thus, equilibrium between the two configurations is anticipated with ∼87% of all species having 5 waters in the equatorial plane and ∼13% having 4 waters according to the Boltzmann factor (Table 3). In stark contrast, the penta-aquo species is highly disfavored for NpO_2^+ and PuO_2^+. In fact, the 5-coordinate plutonyl monocation could not be optimized without migration of the fifth water into the second solvation shell. These data support the gas-phase electrospray observations and complementary DFT calculations recently reported by Rios and coworkers[77] for gas-phase neptunyl and plutonyl; however, it is possible that the proposed equilibrium between aqueous $UO_2(H_2O)_4^+$ and $UO_2(H_2O)_5^+$ may get shifted to favor the 4-coordinate species during the electrospray process.

CONCLUSIONS

DFT calculations employing a benchmarked solution-phase computational protocol and using large hydrated clusters of U, Np, and Pu in the III−VI oxidation states have been performed so as to elucidate the most likely solvation environment in aqueous solution and potential equilibria therein. Assignment of the first solvation shell of these ions is an essential starting point toward understanding their reaction dynamics and complex speciation in aqueous conditions relevant to the nuclear fuel cycle, separations, and environmental remediation. This work is unique among the prior literature reports as three criteria have been used to assign structure of these ions in aqueous solution: (1) accurate solution-phase free energies of solvation and water addition to the first solvation shell, (2) geometrical parameters (metal−oxygen bond lengths), and (3) simulated XANES spectra. Tetravalent U is proposed to exist in equilibrium between the 8- and 9-coordinate species, with the latter being dominant in solution. Moving to the right of the period, Np(IV) and Pu(IV) exist solely as the $Pu(H_2O)_8^{4+}$ species. Reduction of these ions to form the trivalent ions leads to distinct thermodynamic favorability for the octa-aqua species, whose features also lead to excellent reproduction of the XANES spectra. The actinyl dications (AnO_2^{2+}) of U and Np have a preferred environment in the equatorial plane consisting of 5 solvating waters; however, changes to the ionic radius and electronic structure at Pu leads to an equilibrium between the 4- and 5-coordinate species for PuO_2^{2+}. Reduction of the diyl dications to form the monocations generally leads to a preference for the 4-coordinate primary solvation shell, with an equilibrium existing for uranyl, and while the neptunyl and plutonyl species existing solely as $AnO_2(H_2O)_4^+$. These data provide accurate aqueous-phase thermodynamic information for several rare species and reveal trends in hydration behavior across actinide oxidation states and within the early actinide period.

ASSOCIATED CONTENT

Supporting Information

Input parameters for XANES simulations, thermodynamic cycle for obtaining the free energy of solvation, simulated XANES spectra of actinyls, and Cartesian coordinates of all species studied in this work. The Supporting Information is available free of charge on the ACS Publications website at DOI: 10.1021/acs.inorgchem.5b00365.

AUTHOR INFORMATION

Corresponding Author

*E-mail: auclark@wsu.edu.

Notes

The authors declare no competing financial interest.

ACKNOWLEDGMENTS

This work was supported by a grant from the Department of Energy, Basic Energy Sciences, Heavy Element program (DE-SC0001815). S.L. acknowledges the PHY-0649023 Research for Undergraduates program, sponsored by the National Science Foundation. This research used resources of the Oak Ridge Leadership Computing Facility located in the Oak Ridge National Laboratory, which is supported by the Office of Science within the Department of Energy under Contract DE-AC05-00OR22725. The authors thank Dr. Marco Caricato

DOI: 10.1021/acs.inorgchem.5b00365
Inorg. Chem. 2015, 54, 6216−6225

(Gaussian, Inc.) for thoughtful discussion regarding the performance of polarizable continuum models.

REFERENCES

(1) Choppin, G. R.; Rizkalla, E. N. Solution Chemistry of Actinides and Lanthanides. In *Handbook on the Physics and Chemistry of Rare Earths*; Gschneidner, K. A., Jr., Eyring, L., Eds.; North Holland: Amsterdam, **1994**; Vol. *18*, Chapter 128, p 529.
(2) Knope, K. E.; Soderholm, L. *Chem. Rev.* **2013**, *113*, 944−994.
(3) Conradson, S. D.; Al Mahamid, I.; Clark, D. L.; Hess, N. J.; Hudson, A. E.; Neu, M. P.; Palmer, P. D.; Runde, W. H.; Tait, C. D. *Polyhedron* **1998**, *17*, 599−602.
(4) Allen, P. R.; Bucher, J. J.; Shuh, D. K.; Edelstein, N. M.; Craig, I. *Inorg. Chem.* **2000**, *39*, 595−601.
(5) Moll, H.; Danecke, M. A.; Jaliehvand, F.; Sandstrom, M.; Grenthe, I. *Inorg. Chem.* **1999**, *38*, 1795−1799.
(6) Allen, P. G.; Bucher, J. J.; Shuh, D. K.; Edelstein, N. M.; Reich, T. *Inorg. Chem.* **1997**, *36*, 4676−4683.
(7) Neuefeind, J.; Soderholm, L.; Skanthakumar, S. *J. Phys. Chem. A* **2004**, *108*, 2733−2739.
(8) Hudson, E. A.; Allen, P. G.; Terminello, L. J.; Denecke, M. A.; Reich, T. *Phys. Rev. B* **1996**, *54*, 156−165.
(9) Ikeda-Ohno, A.; Hennig, C.; Rossber, A.; Funke, H.; Schelnost, A. C.; Berhnhard, G.; Yalta, T. *Inorg. Chem.* **2008**, *47*, 8294−8305.
(10) Hennig, C. *Phys. Rev. B* **2007**, *75*, 035120.
(11) Antonio, R.; Soderholm, L.; Williams, C. W.; Blaudeau, J.-P.; Bursten, B. E. *Radiochim. Acta* **2001**, *89*, 17−25.
(12) Conradson, S. D. *Appl. Spectrosc.* **1998**, *52*, 252A−279A.
(13) Bratsch, S. G.; Lagowski, J. J. *J. Phys. Chem.* **1986**, *90*, 307−312.
(14) Morss, L. R. *Chem. Rev.* **1976**, *76*, 827−841.
(15) Fuget, J.; Oetting, F. *The Chemical Thermodynamics of Actinide Elements and Compounds, Part 2*; International Atomic Energy Agency: Vienna, 1976.
(16) Fuget, J. In *Actinides in Perspective*; Edelstein, N. M., Ed.; Pergamon Press: New York, 1982; p 409.
(17) David, F. H.; Vokhmin, V. *New. J. Chem.* **2003**, *27*, 1627−1632.
(18) Blaudeau, J.-P.; Zygmunt, S. A.; Curtiss, L. A.; Reed, D. T.; Bursten, B. E. *Chem. Phys. Lett.* **1999**, *310*, 347−354.
(19) Cao, Z.; Balasubramanian, K. *J. Chem. Phys.* **2005**, *123*, 114309.
(20) Gutowski, K. E.; Dixon, D. A. *J. Phys. Chem. A* **2006**, *110*, 8840−8856.
(21) Shamov, G. A.; Schreckenbach, G. *J. Phys. Chem. A* **2005**, *109*, 10961−10974; **2006**, *110*, 12072.
(22) Tsushima, S.; Suzuki, A. *J. Mol. Struct.: THEOCHEM* **2000**, *529*, 21−25.
(23) Tsushima, S.; Yang, T. *Chem. Phys. Lett.* **2005**, *401*, 68−71.
(24) Yang, X.; Liang, Y.; Ding, S.; Li, S.; Chai, Z.; Wang, D. *Inorg. Chem.* **2014**, *53*, 7848−7860.
(25) Odoh, S.; Schreckenbach, G. *J. Phys. Chem. A* **2011**, *115*, 14110−14119.
(26) Heinz, N.; Zhang, J.; Dolg, M. *J. Chem. Theory Comput.* **2014**, *10*, 5593−5598.
(27) Parmar, P.; Samuels, A.; Clark, A. E. *J. Chem. Theory Comput.* **2015**, *11*, 55−63.
(28) Dinescu, A.; Clark, A. E. *J. Phys. Chem. A* **2008**, *112*, 11198.−11206.
(29) Kuta, J.; Clark, A. E. *Inorg. Chem.* **2010**, *49*, 7808−7817.
(30) Rappe, A. K.; Casewit, C. J.; Colwell, K. S.; Goddard, W. A., III.; Skiff, W. M. *J. Am. Chem. Soc.* **1992**, *114*, 10024−10035.
(31) Reich, T.; Bernhard, G.; Geipel, G.; Funke, H.; Hennig, C.; Rossberg, A.; Matz, W.; Schell, N.; Nitsche, H. *Radiochim. Acta* **2000**, *88*, 633−637.
(32) Reich, T.; Geipel, G.; Funke, H.; Hennig, C.; Roβberg, A.; Bernhard, G. *Biannual Report 1999/2000, Project-Group ESRF-Beamline (ROBL-CRG), FZR-322*; ESRF: Grenoble, France, 2001; pp 27−32.
(33) Valiev, M.; Bylaska, E. J.; Govind, N.; Kowalski, K.; Straatsma, T. P.; van Dam, H. J. J.; Wang, D.; Nieplocha, J.; Apra, E.; Windus, T. L.; de Jong, W. A. *Comput. Phys. Commun.* **2010**, *181*, 1477−1660.
(34) Becke, A. D. *J. Chem. Phys.* **1993**, *98*, 5648−5652.
(35) Lee, C.; Yang, W.; Parr, R. G. *Phys. Rev. B* **1988**, *37*, 785−789.
(36) Kuchle, W.; Dolg, M.; Stoll, H.; Preuss, H. *J. Chem. Phys.* **1994**, *100*, 7535−7542.
(37) Dunning, T. H. J. *J. Chem. Phys.* **1989**, *90*, 1007−1023.
(38) Clavaguera-Sarrio, C.; Vallet, V.; Maynau, D.; Marsden, C. J. *J. Chem. Phys.* **2004**, *121*, 5312−5320.
(39) Garcia-Hernandez, M.; Lauterbach, C.; Krüger, S.; Matveev, A.; Rösch, N. *J. Comput. Chem.* **2002**, *23*, 834−846.
(40) Rehr, J. J.; Albers, R. C. *Rev. Mod. Phys.* **2000**, *72*, 621−654.
(41) Rehr, J. J.; Kas, J. J.; Prange, M. P.; Sorina, A. P.; Takimoto, Y.; Vila, F. *C. R. Phys.* **2008**, *10*, 548−559.
(42) Ankudinov, A. L.; Conradson, S. D.; de Leon, J. M.; Rehr, J. J. *Phys. Rev. B* **1998**, *57*, 7518−7525.
(43) Frisch, M. J.; et al. *Gaussian 03*, Revision C.02; Gaussian, Inc.: Wallingford, CT, 2004.
(44) Asthagiri, D.; Pratt, L. R.; Ashbaugh, H. S. *J. Chem. Phys.* **2003**, *119*, 2702−2708.
(45) Ben-Naim, A. *J. Phys. Chem.* **1987**, *82*, 792−803.
(46) Kvamme, B.; Wander, M. C. F.; Clark, A. E. *Int. J. Quantum Chem.* **2009**, *109*, 2474−2481.
(47) Foster, J. P.; Weinhold, F. *J. Am. Chem. Soc.* **1980**, *102*, 7211−7218.
(48) Reed, A. E.; Curtiss, L. A.; Weinhold, F. *Chem. Rev.* **1988**, *88*, 899−926.
(49) Frisch, M. J.; et al. *Gaussian 09*, Revision D.01; Gaussian, Inc.: Wallingford, CT, 2009.
(50) Clark, A. E.; Sonnennberg, J.; Hay, P. J.; Martin, R. L. *J. Chem. Phys.* **2004**, *121*, 2563−2570.
(51) Neck, V.; Kim, J. I. *Radiochim. Acta* **2001**, *89*, 1−16.
(52) Chaboy, J.; Diaz-Moreno, S. *J. Phys. Chem. A* **2011**, *115*, 2345−2349.
(53) Rykov, A. G.; Andreichuk, N. N.; Vasil'ev, V. Y. *Soviet Radiochem. (Engl. Transl.)* **1973**, *15*, 350−355.
(54) Vasil'ev, V. Y.; Andreichuk, N. N.; Rykov, A. G. *Soviet Radiochem. (Engl. Transl.)* **1974**, *16*, 583−586.
(55) Pocev, S.; Johansson, G. *Acta Chem. Scand.* **1973**, *27*, 2146−2160.
(56) Charpin, P.; Dejean, A.; Folcher, G.; Rigny, P.; Navaza, P. J. *J. Chim. Phys. Phys.-Chim. Biol.* **1985**, *82*, 925−931.
(57) Moll, H.; Farkas, I.; Jalilehvand, F.; Sandstrom, M.; Szabo, Z.; Grenthe, I.; Denecke, M. A.; Wahlgren, U. In *Speciation Techniques and Facilities for Radioactive Materials at Synchroton Light Sources*; Nuclear Energy Agency: Organization for Economic Co-operation and Development: Grenoble, France, 1998; pp 261−269.
(58) Frick, R.; Pribil, A. B.; Hofer, T. S.; Randolf, B. R.; Bhattacharjee, A.; Rode, B. M. *Inorg. Chem.* **2009**, *48*, 3993−4002.
(59) Atta-Fynn, R.; Johnson, D. F.; Bylaska, E. J.; Ilton, E. S.; Schenter, G. K.; de Jong, W. A. *Inorg. Chem.* **2012**, *51*, 3016−3024.
(60) Perdew, J. P.; Burke, K.; Ernzerhof, M. *Phys. Rev. Lett.* **1996**, *77*, 3865−3868.
(61) Perdew, J. P.; Burke, K.; Ernzerhof, M. *Phys. Rev. Lett.* **1997**, *78*, 1396.
(62) Horowitz, S. E.; Marston, J. B. *J. Chem. Phys.* **2011**, *134*, 064510.
(63) Odoh, S. O.; Bylaska, E. J.; de Jong, W. A. *J. Phys. Chem. A* **2013**, *117*, 12256−12267.
(64) Gibson, J. K.; Haire, R. G.; Santos, M.; Marçalo, J.; Pires de Matos, A. *J. Phys. Chem. A* **2005**, *109*, 2768−2781.
(65) David, F. H.; Fourest, B.; Hubert, S.; Revel, R.; Auwer, C. D.; Madic, C.; Morss, L. R.; Ionova, G.; Mikhalko, V.; Vokhmin, V.; Nikonov, M.; Berthet, J. C.; Ephritikhine, M. In *Speciation, Techniques and Facilities for Radioactive Materials at Synchrotron Light Sources*; Nuclear Energy Agency: Organisation for Economic Cooperation and Development: Grenoble, France, 1998; pp 95−100.
(66) Mochizuki, Y.; Tsushima, S. *Chem. Phys. Lett.* **2003**, *372*, 114−120.
(67) Wiebke, J.; Moritz, A.; Cao, X.; Dolg, M. *Phys. Chem. Chem. Phys.* **2007**, *9*, 459−465.

DOI: 10.1021/acs.inorgchem.5b00365
Inorg. Chem. 2015, 54, 6216−6225

(68) Vallet, V.; Macak, P.; Wahlgren, U.; Grenthe, I. *Theor. Chem. Acc.* **2006**, *115*, 145−152.
(69) Wahlren, U.; Moll, H.; Grenthe, I.; Schimmelpfennig, B.; Maron, L.; Vallet, V.; Gropen, O. *J. Phys. Chem. A* **1992**, *103*, 8257−8264.
(70) Spencer, S.; Gagliardi, L.; Handy, N. C.; Ioannou, A. G.; Skylaris, C.-K.; Willetts, A.; Simper, A. M. *J. Phys. Chem. A* **1999**, *103*, 1831−1837.
(71) Hay, P. J.; Martin, R. L.; Schreckenbach, G. *J. Phys. Chem. A* **2000**, *104*, 6259−6270.
(72) Cotton, S. *Lanthanide and Actinide Chemistry*; John Wiley and Sons: Chichester, England, 2006.
(73) Shannon, R. D. *Acta Crystallogr.* **1976**, *A32*, 751−767.
(74) Harris, W. E.; Kolthoff, I. M. *J. Am. Chem. Soc.* **1946**, *67*, 1484−1490.
(75) Steele, H.; Taylor, R. J. *Inorg. Chem.* **2007**, *46*, 6311−6318.
(76) Hindman, J. C.; Magnusson, L. B.; LaChapelle, T. J. *J. Am. Chem. Soc.* **1949**, *71*, 687−693.
(77) Rios, D.; Michelini, M. C.; Lucena, A. F.; Marçalo, J.; Bray, T. H.; Gibson, J. K. *Inorg. Chem.* **2012**, *51*, 6603−6614.

DOI: 10.1021/acs.inorgchem.5b00365
Inorg. Chem. 2015, 54, 6216−6225